

Experimental determination of three-dimensional finite-time Lyapunov exponents in multi-component flows

Samuel G. Raben · Shane D. Ross ·
Pavlos P. Vlachos

Received: 3 July 2014 / Revised: 1 September 2014 / Accepted: 5 September 2014
© Springer-Verlag Berlin Heidelberg 2014

Abstract We present an experimental approach for estimating finite-time Lyapunov exponent fields (FTLEs) in three-dimensional multi-component or multi-phase flows. From time-resolved sequences of particle images, we directly compute the flow map and coherent structures, while avoiding and outperforming the computationally costly numerical integration. Performing this operation independently on each flow component enables the determination of three-dimensional Lagrangian coherent structures (LCSs) without any bias from the other components. The locations of concurrent LCSs for different flow elements (e.g., passive tracers, inertial particles, bubbles, or active particles) can provide new insight into the interpenetrating FTLE structure in complex flows.

Finite-time Lyapunov exponents (FTLEs) are an increasingly popular tool for describing mixing and transport in complex flow fields (Haller 2001; Brunton and Rowley 2010). FTLEs provide a measure of the exponential rate of divergence or convergence of Lagrangian particle trajectories. They can be used both experimentally and numerically to describe a flow field, which may have a high

degree of spatiotemporal complexity (Haller 2001; Shadden et al. 2006, 2007). While FTLEs are primarily used to describe single-phase flow behavior (Haller 2001, 2005; Shadden et al. 2006), some works have attempted to account for inertial particles by modeling the particles' motion through simulations (Haller and Sapsis 2008; Tallapragada and Ross 2008; Peng and Dabiri 2009). This procedure can provide insight, but does not provide direct information about the true observable inertial particle trajectories. Often, the equations for inertial particle motion make simplifying assumptions (e.g., the Maxey–Riley equations; Maxey 1983) that can lead to significant differences between the modeled and true motion. This brief communication describes a method to directly determine FTLEs from experimental data for inertial particles through the use of particle tracking velocimetry (PTV) without any a priori assumptions about particle motion.

FTLEs are computed via the Cauchy-Green deformation tensor C_{jk} ,

$$C = \left(\nabla \Phi_{t_0}^{t_0+T} \right)^* \cdot \nabla \Phi_{t_0}^{t_0+T} \quad (1)$$

where $*$ denotes the matrix transpose, $\Phi_{t_0}^{t_0+T}$ is the flow map (diffeomorphism) of particle locations from time t_0 to $t_0 + T$, and T is the duration over which the FTLEs will be computed and can be positive or negative, corresponding to forward or backward FTLE, respectively. From the maximum eigenvalue of C , the FTLE field defined in the measurement volume is,

$$\sigma_{t_0}^{t_0+T} = \frac{1}{|T|} \ln \left(\sqrt{\lambda_{\max}(C)} \right) \quad (2)$$

It is typical when computing FTLEs from experimental data to use a numerical integration routine to numerically advect artificial tracer particles to determine the flow map

S. G. Raben
School of Physics, Georgia Tech, Atlanta, GA, USA
e-mail: sam.rabeh@gmail.com

S. D. Ross
Biomedical Engineering and Mechanics, Virginia Tech,
Blacksburg, VA, USA
e-mail: sdross@vt.edu

P. P. Vlachos (✉)
Mechanical Engineering, Purdue University, West Lafayette, IN,
USA
e-mail: pvlachos@purdue.edu

from the estimated velocity field (Shadden et al. 2006, 2007; Lekien and Ross 2010). While this can be effective for single-phase flow, it neglects the fact that inertial particles, bubbles, or active particles may fail to follow the bulk fluid motion or the fact that tracking individual particles can provide a direct measure of a short duration flow map. Lagrangian tracking can provide a measure of the flow map over longer times but is more prone to experimental errors (Raben et al. 2014). While numerical routines can be modified to estimate the inertial particle behavior via modeling as mentioned above, this procedure does not directly measure inertial particle trajectories. However, using time-resolved PTV to obtain snap shots of the particle motion allows direct measurement of the particle flow map while also allowing for parameterization of the particle flow map based on unique identifying characteristics, such as size, shape, or color, providing, e.g., a one-parameter family of particle flow maps with particle size as the parameter. The concept of merging small flow map snap shots to estimate a complete flow map was put forth by Brunton and Rowley (2010) for results of fluid computations and later adapted for experimental data as PTV interpolation by Raben et al. (2014). Through this method it is possible to simultaneously determine FTLEs for multiple particle groups within the same measurement volume and compare them to the bulk flow field. It has also been shown that this method can provide high-accuracy flow map computation results even when the particle concentration drops below what is typically used for PIV/PTV (Raben et al. 2014). While this work did not determine a lower limit for seeding, it did outperform all other tested methods for very low particle concentrations. Ultimately, seeding density in these multi-component environments will depend on the type of flow and the interplay of velocity time and length scales and the mean inter-particle separation. The ability to resolve low seeding density is an important feature; when the particles are separated into groups, some groups will have smaller particle population densities requiring a method suitable to provide high-resolution FTLE information with low-resolution velocity information in order to properly determining the FTLE values.

To study the motion of inertial particles in an experimental environment, data were collected in a vertical water tunnel that was designed to generate homogeneous isotropic grid turbulence, as described in Raben et al. (2012). The Reynolds number for this facility, based on the hydraulic diameter, was 8,738 with particles moving roughly 2 voxels (within the volume of interest) per frame pair. For this experiment, a bar thickness of the grid, $b = 0.3175$ cm, was used with the gap between bars equal to the width of the bar. Overlapping bars created a square lattice, which was located 8-cm upstream from the

measurement location. Two different types of particles were added to the flow: 85 ± 20 μm -diameter silver-coated hollow glass spheres that were tuned to be neutrally buoyant and were used to act as flow tracers; solid glass particles with diameters ranging from approximately 150–200 μm that were added downstream (top of the tunnel) and had an approximate mass density of 2,600 kg/m^3 . The vertical nature of the tunnel created opposing motion as gravity pulled the negatively buoyant particles down, while the bulk flow was moving mostly upward.

Time-resolved imaging techniques such as particle image velocimetry (PIV) have made it possible to study the Lagrangian motion of a flow field experimentally (Mathur et al. 2007; Shadden et al. 2007). With the recent development of volumetric image techniques (Elsinga et al. 2006), it is now possible to investigate particle trajectories in a fully three-dimensional flow field. Because these imaging techniques make no assumptions on particle motion (e.g., must be a tracer following the bulk flow), they can be effective in capturing non-flow tracer particle motion (e.g., inertial particles) as well as bulk flow motion.

Time-resolved tomographic imaging was used to collect information on the complete particle field as well as fully resolve the three-dimensional fluid motion. A New Wave Pegasus laser was used to illuminate all the particles in the measurement volume. Three Photron FASTCAM APX-RS high-speed CMOS cameras were used to simultaneously image this light field, recording images at 250 Hz. These images were reconstructed into a three-dimensional light intensity distribution using the multiplicative algebraic reconstruction technique (MART) using the Lavisision DaVis 8.1 software (Herman and Lent 1976; Elsinga et al. 2006).

Once the images had been reconstructed, the particles' size and motion were determined. Particles were first located in the volume using a simple thresholding method and then sized using an intensity weighted pixel count. In an effort to track the particles, a multi-component particle tracking algorithm developed for single- and multi-phase flows (Cardwell et al. 2011) was adapted to three-dimensional data. The method performs the tracking by comparing a set of unique particle identifiers, such as size, peak intensity, and proximity, and matches particles in consecutive images by minimizing a weighted function of these parameters. This method has been shown to work well in turbulent flows even with non-flow tracer particles (Cardwell et al. 2011).

Figure 1a shows a histogram of the particle sizes present in the measurement volume. Due to factors such as camera arrangement and the MART reconstruction algorithm (Herman and Lent 1976), the particle size may be over-estimated. As these factors should affect all particles equally, and the concern here is not the exact particle size

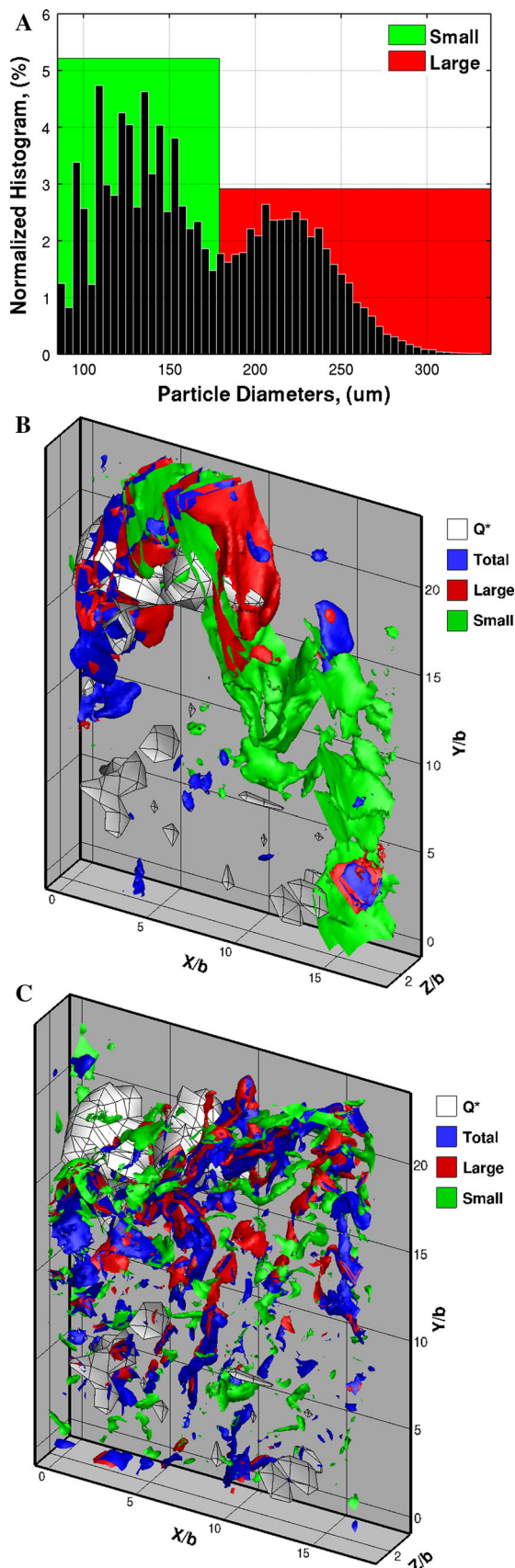


Fig. 1 a Normalized particle diameter distribution within the measurement volume. Iso-surfaces of the forward (b) and backward (c) FTLE fields based on the different components in the flow

but rather their relative size, this should not affect the results. For this study, the particle size distribution was divided into two groups. The first group was composed of the smaller particles, most likely silver-coated spheres, which should follow the bulk fluid motion. The second group was composed of the large particles, which were primarily large glass particles that would tend not to follow the bulk fluid motion. When computing the FTLE field, the complete particle distribution was used as a control, as this total group provides an estimate of the FTLE field that would be found if no particle sizing procedure had been applied to the data, and all the particles were (erroneously) treated as flow tracers.

The FTLE field was calculated for each particle group with an integration time of 0.211τ (where τ is a characteristic timescale given by the hydraulic diameter divided by the channel velocity) which is equal to 250 frame pairs. For flows in two-dimensional domain, FTLE fields are often characterized by the elevated ridges, or connected lines with high FTLE values, which are referred to as Lagrangian coherent structures (LCSs) and reveal hyperbolic or shear-dominated structures. In three-dimensional domains, the loci of elevated values are two-dimensional surfaces. Figure 1b, c shows iso-surface of high FTLE values as proxies for true ridges for both the forward and backward FTLE fields with the threshold set equal to one over the integration time. For consistency, the threshold was maintained constant between the two fields. Ridges in the forward FTLE field reveal repelling surfaces where particles are exponentially diverging away from one another, while the backward FTLE shows attracting surfaces where particles are exponentially converging and may be related to clustering cores for inertial particles. From Fig. 1b, it can be seen that there is a significant difference in the FTLE fields based on the particle size. The iso-surface for the large particle group is dominated by a large structure in the upper left of the domain. It could be seen from the raw data that during this time, there was an influx of larger particles that begin to spread throughout the volume, which would explain the elevated FTLE values in this region. For the small particle group, the iso-surface shows a structure that extends from the lower right of the domain up to the top. This structure could indicate that the influx of large particles forced the flow tracers to be redirected around the large particle cluster causing a divergence in the small particle trajectories.

Figure 1c shows the backward FTLE, which will indicate locations of particle clustering. Previous studies that

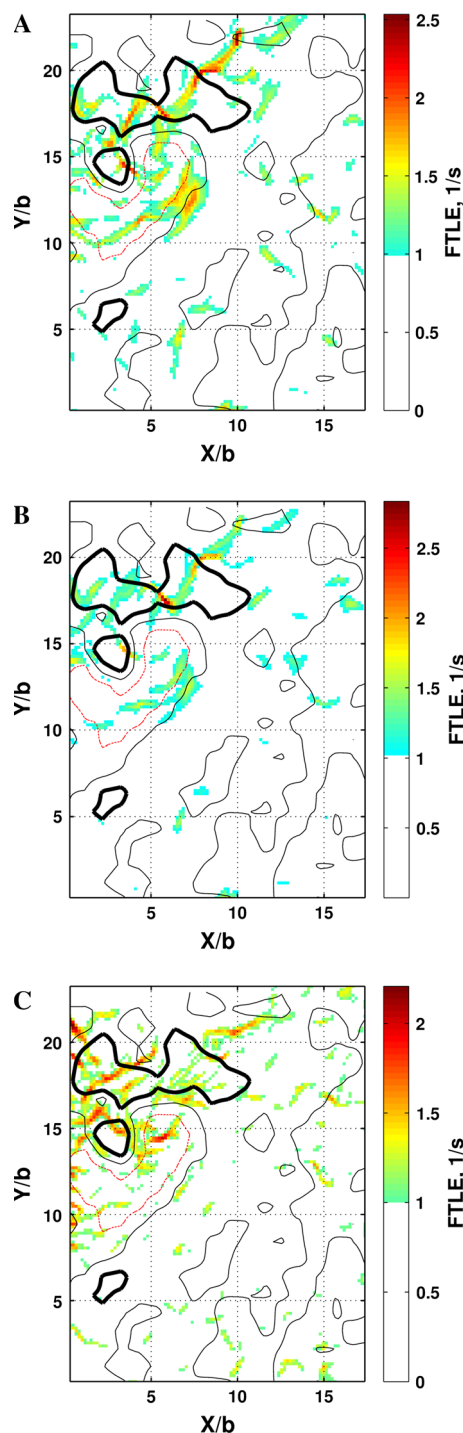


Fig. 2 Contours of backward time FTLE values for the total location of particles **a**, the large particle sizes **b**, and finally, the small particle sizes, **c**. The *thick line* shows iso-contour for -3 standard deviations (surface shown in Fig. 1b, c), while the *thick line* shows an iso-contour for -1.5 standard deviations and the *dashed line* is the zero iso-contour

have investigated particle clustering have used the second invariant of the velocity gradient tensor, Q , sometimes referred to as the Okubo–Weiss parameter, as an indicator

for where particles are likely to concentrate (Squires and Eaton 1991; Eaton 1994; Guala et al. 2008; Haller and Sapsis 2008), where Q is defined as,

$$Q = \frac{1}{2}(\omega^2 - s^2) \quad (3)$$

with ω and s representing vorticity and strain rate, respectively. For scaling purposes, Q is often normalized by the ensemble average of vorticity squared, $Q^* = Q/\langle\omega^2\rangle$, as was done here. This produced normalized values between -1.5 and 0.5 which is in agreement with the literature for turbulent flow Guala et al. (2008). When $Q^* < 0$, this indicates a region of high strain and low vorticity, sometimes referred to as saddle-like regions, since this classification, Eulerian in nature, is justified only near stagnation points of steady flows (Basdevant and Philipovitch 1994) [away from stagnation points, the criterion has been shown to be incorrect (Haller and Yuan 2000)]. Only instantaneous flow structures can be identified via Q^* , which are not generally relevant to finite-time transport as experimental flow fields are generally unsteady (time dependent). Nonetheless, when particles are added to the flow, the $Q^* < 0$ regions have been shown to correlate with preferential particle concentration (Squires and Eaton 1991; Eaton 1994; Guala et al. 2008; Haller and Sapsis 2008). To illustrate regions where particles should cluster according to the Q^* criteria, Q^* iso-surfaces are also given in Fig. 1, showing the location of three standard deviations away from the zero in the negative direction based on the mean field. It can be seen from Fig. 1c that while there exist some smaller regions of high backward FTLE throughout the domain, the attracting LCS locations are predominantly located near the location of higher negative Q^* .

Since the flow is time dependent, there is no reason to expect perfect agreement between the Eulerian Q^* field. While Q^* is computed a discrete locations in space for a fixed time instant, the LCSs are computed using the temporal evolution of the moving particles.

To further investigate the locations of particle clustering, Fig. 2 shows backward FTLE values on the center Z plane for each of the two different particle groupings along with the total particle collection, with a thick black line representing the same iso-contour of Q^* is included. In addition, an iso-contour -1.5 times the standard deviation and a zero contour are also included. It can be seen from this figure that while there are some similarities in the locations of the elevated backward FTLE values between the different groups, there are also some important differences. Figure 2a shows the FTLE field for the total particle group, which we note is not a superposition of the FTLE field for the size-based groups. Elevated FTLE values are seen in close proximity to the highly negative Q^* values, as

this will be a location where particles will cluster (Guala et al. 2008). For the large particles, Fig. 2b, elevated values are again seen near highly negative Q^* but in a different location from that seen with the total particle group. In this case, the large particles appear to be more closely packed around the region of highly negative Q^* . The large particles also have a lower maximum FTLE value, which may indicate that their attraction to this region is not as strong as some of the other particles groups.

For the small particles, Fig. 2c, it can again be seen that the elevated FTLE values are located near the Q^* iso-contour. This particle group appears to have more scatter than the other groups which is mostly due to the fact that as flow tracers these particles are more susceptible to the turbulent fluctuations in the volume and thus will have a more spatially distributed structure. Again, because Q^* is an Eulerian field and ours is a temporally varying flow, there is no expectation of perfect agreement with the LCS, but it does help to illustrate the behavior. It can also be seen from this figure that the average FTLE value appears higher than that of the large particles which is in agreement with previous numerical works (Bec et al. 2006).

Because of the variation in Stokes numbers between the different particle groups, the FTLE fields that are produced are different. The different Stokes numbers of each particle group, and by extension their temporal response, mean that the different particle groups will be effected by different scales of the flow. The smaller particles will be more directly influenced by small-scale flow structures, while the larger particles will be more ballistic and likely to respond to the large-scale features. This increased temporal response in the smaller particles will translate to more small-scale structure in the FTLE field as the exponential divergence occurs more rapidly (Fig. 2). Because these fields are generated from Lagrangian information, it can be expected that they will not be exactly the same as fields generated using only Eulerian information, i.e., the Q^* field. An important aspect of the approach presented here is that it enables the data to reveal the locations at which the different FTLE fields, which are computed using particles with different sizes, do overlap. These different fields are unique to each particle group and thus can only be obtained, as introduced here, through computing the FTLE fields separately through particle tracking. These overlapping structures denote the inter-penetration of the FTLE fields, which subsequently can be used to identify locations of global attraction (or repulsion in the case of forward time FTLEs) for this range of particle sizes. Because inertial particles by definition will not be perfect flow tracers, it is important to remember that they will define a different FTLE field then their flow tracer counterparts (Tallapragada and Ross 2008).

We posit that analyzing where these fields overlap can potentially provide a novel parameter for describing the dynamics of the flow field and may provide insight into the stability of transport barriers which in turn adds to their importance in describing the overall transport of the field.

In summary, this work has shown that three-dimensional FTLE fields can be calculated for inertial particles in experiments through the use a non-flow tracer flow map determination technique that uses particle tracking and sizing information to directly measure the size-parameterized families of flow maps. The use of particle tracking for the direct calculation of the three-dimensional FTLEs is an important advancement, as it is capable of uniquely determining the flow maps for different groups of particles, e.g., grouped by size in our experiment, but other parameterizations are possible. Using this method, it is possible to directly measure inertial particle FTLE fields and Lagrangian coherent structures without making assumptions about the underlying particle equations of motion. This work also enables the calculation of inter-penetrating FTLE fields for different particle groups. Inter-penetration of FTLE fields from different particle groups may indicate locations of global attraction or repulsion which would increase our insight for multi-component and multi-phase flow and transport processes.

Acknowledgments SDR gratefully acknowledges partial support from NSF Grant 1150456.

References

- Basdevant C, Philipovitch T (1994) On the validity of the “Weiss criterion” in two-dimensional turbulence. *Phys D Nonlinear Phenom* 73(1):17–30
- Bec J, Biferala L, Boffetta G, Cencini M, Musacchio S, Toschi F (2006) Lyapunov exponents of heavy particles in turbulence. *Phys Fluids* 18. <http://scitation.aip.org/content/aip/journal/pof2/18/9/10.1063/1.2349587>
- Brunton S, Rowley C (2010) Fast computation of finite-time Lyapunov exponent fields for unsteady flows. *Chaos Interdiscip J Nonlinear Sci* 1–12. doi:10.1063/1.3270044. <http://link.aip.org/link/?CHAOEH/20/017503/1>
- Cardwell ND, Vlachos PP, Thole Ka (2011) A multi-parametric particle-pairing algorithm for particle tracking in single and multiphase flows. *Meas Sci Technol* 22(10):105406. doi:10.1088/0957-0233/22/10/105406. <http://stacks.iop.org/0957-0233/22/i=10/a=105406?key=crossref.6646d1e538c3c7e02789a29738af16be>
- Eaton JK (1994) Preferential concentration of particles by turbulence. *Int J Multiph Flow* 20:169. <http://link.aip.org/link/?PFADEB/3/1169/1>
- Elsinga GEGE, Scarano F, Wieneke B, Oudheusden BWV, van Oudheusden BW (2006) Tomographic particle image velocimetry. *Exp Fluids* 41(6):933. doi:10.1007/s00348-006-0212-z
- Guala M, Liberzon A, Hoyer K (2008) Experimental study on clustering of large particles in homogeneous turbulent flow. *J Turbul* 9(34):1. doi:10.1080/14685240802441118

- Haller G (2001) Distinguished material surfaces and coherent structures in three-dimensional fluid flows. *Phys D* 149:248
- Haller G (2005) An objective definition of a vortex. *J Fluid Mech* 525:1. doi:[10.1017/S0022112004002526](https://doi.org/10.1017/S0022112004002526)
- Haller G, Sapsis T (2008) Where do inertial particles go in fluid flows? *Phys D Nonlinear Phenom* 237(5):573–583. doi:[10.1016/j.physd.2007.09.027](https://doi.org/10.1016/j.physd.2007.09.027)
- Haller G, Yuan G (2000) Lagrangian coherent structures and mixing in two-dimensional turbulence. *Phys D* 147:352
- Herman G, Lent A (1976) Iterative reconstruction algorithms. *Comput Biol Med* 6(3):273. <http://www.sciencedirect.com/science/article/pii/0010482576900664>
- Lekien F, Ross SD (2010) The computation of finite-time Lyapunov exponents on unstructured meshes and for non-Euclidean manifolds. *Chaos* 20:017505. doi:[10.1063/1.3278516](https://doi.org/10.1063/1.3278516)
- Mathur M, Haller G, Peacock T, Ruppert-felsot JE, Swinney HL (2007) Uncovering the Lagrangian skeleton of turbulence. *Phys Rev Lett* 98:1. doi:[10.1103/PhysRevLett.98.144502](https://doi.org/10.1103/PhysRevLett.98.144502)
- Maxey MR (1983) Equation of motion for a small rigid sphere in a nonuniform flow. *Phys Fluids* 26(4):883. doi:[10.1063/1.864230](https://doi.org/10.1063/1.864230)
- Peng J, Dabiri JO (2009) Transport of inertial particles by Lagrangian coherent structures: application to predator–prey interaction in jellyfish feeding. *J Fluid Mech* 623:75. doi:[10.1017/S0022112008005089](https://doi.org/10.1017/S0022112008005089)
- Raben SG, Charonko JJ, Vlachos PP (2012) Adaptive gappy proper orthogonal decomposition for particle image velocimetry data reconstruction. *Meas Sci Technol* 23(2):025303. doi:[10.1088/0957-0233/23/2/025303](https://doi.org/10.1088/0957-0233/23/2/025303). <http://stacks.iop.org/0957-0233/23/i=2/a=025303?key=crossref.e5c3fe9270eba84484189ab2ad1c8278>
- Raben SG, Ross SD, Vlachos PP (2014) Computation of finite-time Lyapunov exponents from time-resolved particle image velocimetry data. *Exp Fluids* 55(1):1638. doi:[10.1007/s00348-013-1638-8](https://doi.org/10.1007/s00348-013-1638-8)
- Shadden SC, Dabiri JO, Marsden JE (2006) Lagrangian analysis of fluid transport in empirical vortex ring flows. *Phys Fluids* 18:1
- Shadden SC, Katija K, Rosenfeld M, Marsden JE, Dabiri JO (2007) Transport and stirring induced by vortex formation. *J Fluid Mech* 593:315. doi:[10.1017/S0022112007008865](https://doi.org/10.1017/S0022112007008865)
- Squires K, Eaton J (1991) Preferential concentration of particles by turbulence. *Phys Fluids A Fluid Dyn* 1169(3):5. doi:[10.1063/1.858045](https://doi.org/10.1063/1.858045). <http://link.aip.org/link/?PFADEB/3/1169/1>, <http://link.aip.org/link/PFADEB/v3/i5/p1169/s1&Agg=doi>, <http://scitation.aip.org/content/aip/journal/pofa/3/5/10.1063/1.858045>
- Tallapragada P, Ross SD (2008) Particle segregation by Stokes number for small neutrally buoyant spheres in a fluid. *Phys Rev E* 78:1. doi:[10.1103/PhysRevE.78.036308](https://doi.org/10.1103/PhysRevE.78.036308)